The human phosphorylated pathway: a multienzyme metabolic assembly for L-serine biosynthesis

Valentina Rabattoni[1], Francesco Marchesani[2] (iD), Giulia Murtas[1], Silvia Sacchi[1] (iD), Andrea Mozzarelli[3], Stefano Bruno[2] (iD), Alessio Peracchi[4] (iD), Loredano Pollegioni[1] (iD) and Barbara Campanini[2] (iD)

1 The Protein Factory 2.0, Department of Biotechnology and Life Sciences, University of Insubria, Varese, Italy
2 Department of Food and Drug, University of Parma, Italy
3 Institute of Biophysics, CNR, Pisa, Italy
4 Department of Chemistry, Life Sciences and Environmental Sustainability, University of Parma, Italy

De novo L-serine biosynthesis in the mammalian astrocytes proceeds via a linear, three-step pathway (the phosphorylated pathway) catalysed by 3-phosphoglycerate dehydrogenase (PHGDH), phosphoserine aminotransferase (PSAT) and phosphoserine phosphatase (PSP). The first reaction, catalysed by PHGDH and using the glycolytic intermediate 3-phosphoglycerate, is strongly shifted towards the reagents, and coupling to the following step by PSAT is required to push the equilibrium towards L-serine formation; the last step, catalysed by PSP, is virtually irreversible and inhibited by the final product L-serine. Very little is known about the regulation of the human phosphorylated pathway and the ability of the three enzymes to organise in a complex with potential regulatory functions. Here, the complex formation was investigated in differentiated human astrocytes, by proximity ligation assay, and *in vitro* on the human recombinant enzymes. The results indicate that the three enzymes co-localise in cytoplasmic clusters that more stably engage PSAT and PSP. Although *in vitro* analyses based on native PAGE, size exclusion chromatography and cross-linking experiments do not show the formation of a stable complex, kinetic studies of the reconstituted pathway using physiological enzyme and substrate concentrations support cluster formation and indicate that PHGDH catalyses the rate-limiting step while PSP reaction is the driving force for the whole pathway. The enzyme agglomerate assembly of the phosphorylated pathway (the putative 'serinosome') delivers a relevant level of sophistication to the control of L-serine biosynthesis in human cells, a process strictly related to the modulation of the brain levels of D-serine and glycine, the main co-agonists of *N*-methyl-D-aspartate receptors and various pathological states.

Introduction

L-Serine (L-Ser), referred to as a conditionally nonessential amino acid, plays a versatile role in intermediary metabolism in eukaryotic cells, serving in the production of phosphoglycerides, glycerides, sphingolipids, phosphatidylserine and methylenetetrahydrofolate (a source of one-carbon units for methylation processes and nucleotide synthesis). L-Ser is also the precursor of two neuroactive signalling molecules: glycine and D-serine, which modulate the activity of *N*-methyl-D-aspartate receptors. L-Ser metabolism plays a major role in the development and function of the central nervous system (CNS) [1,2]. Because of the low permeability of L-Ser through the blood–brain barrier, its brain concentration is largely due to biosynthesis through the phosphorylated pathway (PP) in astrocytes [3,4]. This cytosolic pathway starts from 3-phosphoglycerate (3PG, generated by glycolysis) and involves the enzymes 3-phosphoglycerate dehydrogenase (PHGDH, EC1.1.1.95; producing 3-phosphohydroxypyruvate, 3PHP), phosphoserine aminotransferase (PSAT, EC2.6.1.52; producing 3-phosphoserine, 3PS) and phosphoserine phosphatase (PSP, EC3.1.3.3; catalysing the last hydrolytic irreversible step). The final product is L-Ser [5] (see Scheme 1). Since PP is present in most organisms, from bacteria to mammals, extensive literature exists on the functional and structural properties of the enzymes from different sources. For example, both PSP and PSAT from hyperthermophilic bacteria [6,7], *Mycobacterium tuberculosis* [8], plants [9–11] and mammals [12–16] have been characterised to date. In particular, deep investigations have been reported for PHGDH from bacterial sources, highlighting differences and similarities with the human counterpart [5,17].

Severe, infantile, neurological disorders, including congenital microcephaly, intractable seizures and several psychomotor defects have been linked to serine (and glycine) deficiency [18,19]. For example, Neu–Laxova syndrome was identified as a rare, severe and lethal L-Ser deficiency disorder that originates from defects in the genes encoding the enzymes of the PP [20]. Indeed, patients showing a strong decrease in L-Ser and glycine levels in plasma/cerebrospinal fluid are affected by severe neurological disorders. The PP is also linked to cancer, since the hyperactivation of the L-Ser/glycine biosynthetic pathway drives oncogenesis; for a review, see [21]. Furthermore, the PP was recently linked to mechanisms differing between genders in healthy ageing and Alzheimer's disease onset [22].

Interactions between proteins play a central role in biological processes. Homo- and hetero-subunit oligomerisation confers protein stability and extends protein functionality, including enhancing enzyme catalytic rates and bestowing allosteric properties [23-25]. Large protein complexes may serve to shuttle intermediates along a particular pathway, especially when substrates are unstable, to avoid their use by alternative pathways or when they are present at concentrations lower than their cognate enzymes. These are metabolic strategies named 'substrate or direct channelling' [26], made possible via the formation of protein tunnels connecting consecutive active sites [27]. An alternative is represented by 'proximity channelling', which involves two enzymes positioned near enough to each other such that the intermediate produced by the first enzyme is processed by the second enzyme before it can escape by diffusion, even in the absence of an actual channel. The main issue of such a process is the distance between the two enzymes: An intermediate produced by the first enzyme is unlikely to be processed by the second enzyme when the distance between the two active sites is ~ 10 nm apart [28]. An alternative to generate channelling is represented by assembling multiple copies of the involved enzymes into a functional co-cluster, an 'agglomerate' [27]. In this case, once the upstream enzyme produces an intermediate, the probability it will be processed by one of the many copies of the downstream enzyme in the agglomerate is high. An example is represented by the six enzymes of the purine biosynthetic pathway, which form a reversible cluster, named purinosome, in HeLa cells in response to purine availability [29,30]. Interestingly, cell metabolism seems to be localised in nano- and micron-sized
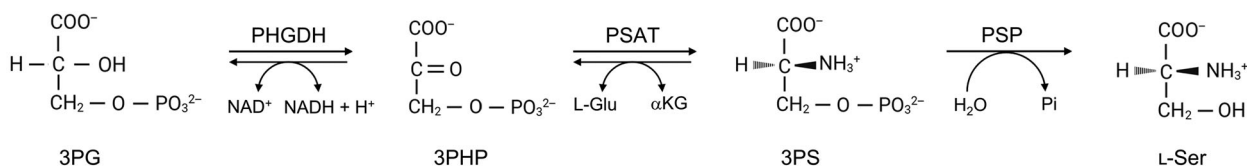
Scheme 1. Scheme of the reactions of the phosphorylated pathway. PHGDH catalyses the NAD$^+$-dependent conversion of D-3-phosphoglycerate into 3-phosphohydroxypyruvate; PSAT catalyses the transamination of 3-phosphohydroxypyruvate to L-3-phosphoserine with glutamate as an amino donor and using a pyridoxal-5'-phosphate cofactor; PSP catalyses the irreversible hydrolysis of L-3-phosphoserine to L-serine.

compartments that coherently assemble protein complexes and thus catalyse, organise and integrate complex pathways.

Recently, the structural and functional properties of the three human enzymes of the PP have been investigated [5,31–33]. Because of the cytosolic location of the PP and its connection with glycolysis (3PG is an intermediate of glycolysis that can be diverted to generate L-Ser), the knowledge of the PP organisation is of primary relevance. In this work, we provide several lines of compelling evidence that the three enzymes of the PP do not form a stable and separable complex. Our results point to the generation of a multienzyme metabolic assembly (an enzyme agglomerate we named 'serinosome') that controls L-Ser synthesis in human cells.

Results
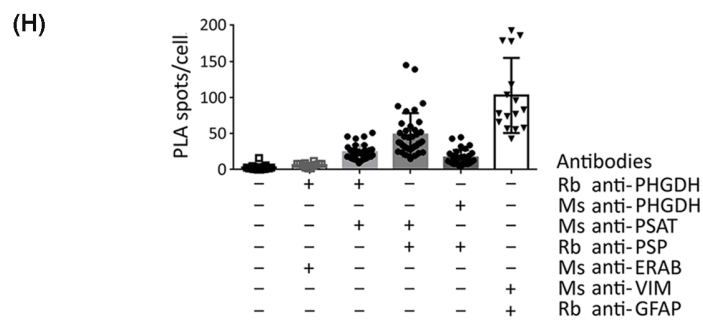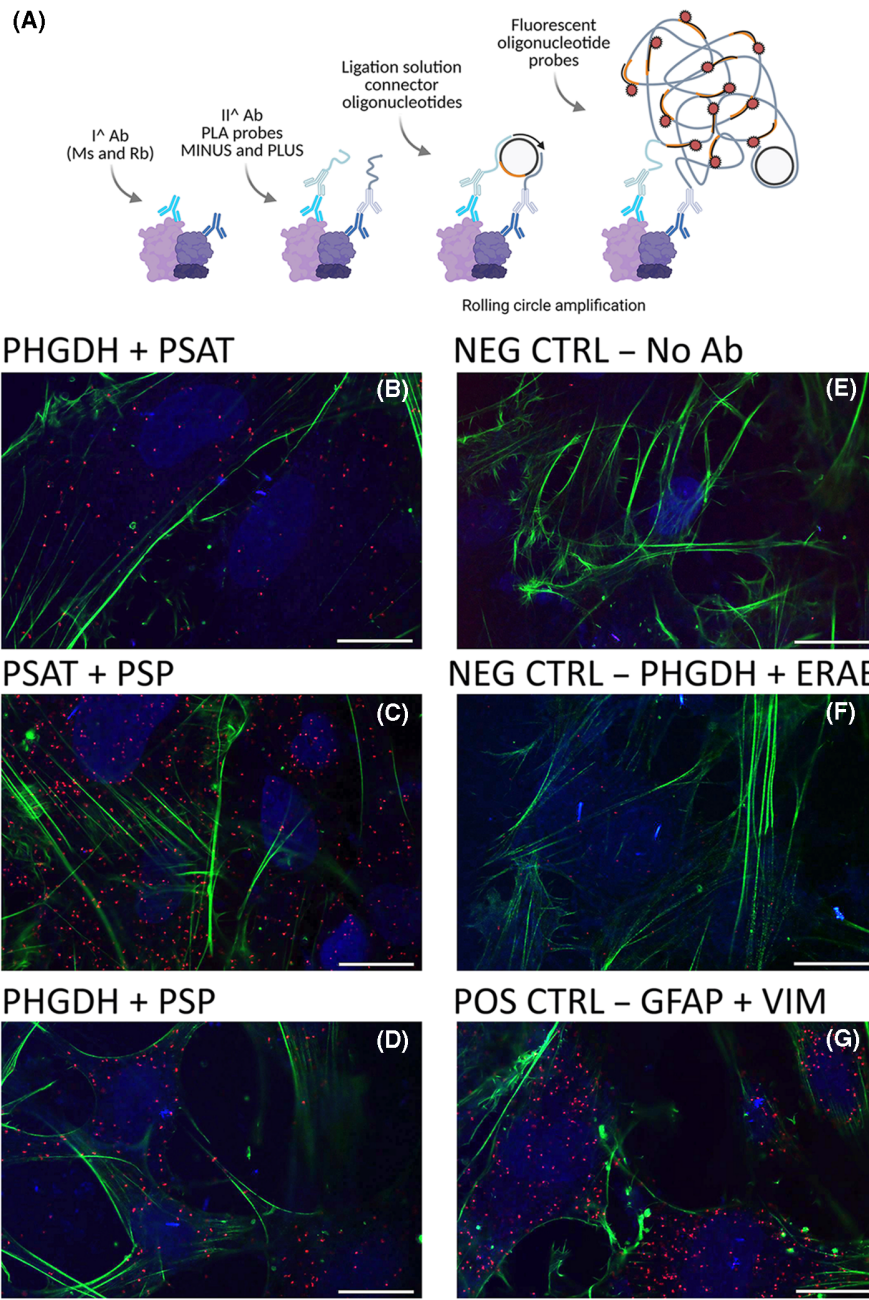
PP complex formation at the cellular level

The ability of the three enzymes of the PP to generate a complex at the cellular level was evaluated by the proximity ligation assay (PLA, also referred to as Duolink technology). We selected this strategy based on its ability to provide a highly specific and sensitive detection of protein–protein interactions at the cell level [34]. In each assay, two primary antibodies (raised from different species and recognising the putative interacting proteins) are used together with species-specific secondary antibodies conjugated to unique short DNA oligonucleotides (Duolink probes), which template the hybridisation of added connector oligonucleotides. When in close proximity (< 40 nm), the oligonucleotides are ligated to form a circular, single-stranded DNA template. This template, still anchored to the antibody, is then subjected to rolling circle amplification (RCA) generating a long concatemer product, which is detected using complementary fluorescent oligonucleotide probes (see the scheme in Fig. 1A). This generates discrete fluorescent dot signals (spot of proximity) that can be counted, showing the exact subcellular location of the protein–protein interaction.

In *p*-formaldehyde-fixed differentiated astrocytes derived from human induced pluripotent stem cells (iPSC) at 30 days of *in vitro* differentiation (30 DIV) (Tripodi F., Motta Z., Murtas G., Rabattoni V., Nonnis S., Grassi Scalvini F., Rinaldi A.M., Rizzi R, Bearzi C., Badone B., Sacchi S., Tedeschi G., Maffioli E., Coccetti P., Pollegioni L, unpublished data), couples of antibodies were used to specifically recognise endogenously expressed PHGDH, PSAT and PSP. These antibodies were recognised by the Duolink probes and, after the hybridisation and RCA steps, PLA signals were detected by confocal microscopy. In the large majority of cells, spots of proximity were detected either when PHGDH and PSAT, or PSAT and PSP, or PHGDH and PSP were labelled (Fig. 1B–D), as observed for glial fibrillary acidic protein (GFAP) and vimentin in the positive control (Fig. 1G), and not for PHGDH and 3-hydroxyacyl-CoA dehydrogenase type II (ERAB) in the negative one (Fig. 1F). This finding strongly suggested that the PP's proteins are interacting. Notably, in differentiated astrocytes the density of the detected signals (expressed as the mean number of PLA spots per cell) is similar to the one reported for other metabolic enzyme assemblies, i.e. the purinosome [35,36]. However, it is significantly higher when the interaction of PSAT with PSP is analysed (Fig. 1H), likely indicating either that fewer PHGDH molecules are engaged in the putative 'serinosome' formation or that this enzyme is less stably associated with the protein cluster, in the experimental condition we used.

In line with the latter observations, double staining immunofluorescence analyses, performed using the same antibody mixtures as in PLA analyses, showed the partial co-occurrence of the signals corresponding to PHGDH and PSAT, PSAT and PSP, and PSP and PHGDH, as indicated by the yellow colocalisation spots in Fig. 2A–C. The actual correlation of red and green signals and the degree of colocalisation of the labelled PP's enzymes were evaluated by the FIJI software using the JACoP plugin, which allows the calculation of several colocalisation coefficients. In particular, Manders' coefficients (M1 and M2) estimated the fluorescent signal (i.e. red channel) overlapping the other one (i.e. green channel): The number of co-occurring pixels as a fraction of the M1 and M2 coefficients, separately for each fluorophore, accounts for the fraction of the total fluorescence that co-occurs. The obtained values (in the 0.47–0.58 range for both M1 and M2, Table 1) indicated that the signals corresponding to the PP's enzymes largely overlap, albeit the colocalisation was not complete.

Besides this, the correlation between red and green signal pairs in sets of single cells was evaluated by the Pearsons' coefficient (r, computed setting a Costes' threshold), a measure of the strength of the linear relationship between the two channels. PHGDH and PSAT, PSAT and PSP, and PSP and PHGDH signals co-distribute: Mean r values corresponding to 0.63 (0.5–0.73 range), 0.60 (0.51–0.68 range) and 0.62 (0.61–0.80 range), respectively, were calculated (Table 1), indicating a fairly high correlation of the signals for the PP's enzymes couples. Altogether, these findings further support the close proximity and the engagement of the PP's proteins in multimeric

Fig. 1. Investigation of the PP's protein interaction at the cellular level. (A) Schematic diagram of Proximity Ligation Assay (see details in the text), created with BioRender.com. (B–D) Astrocytes were probed with rabbit anti-PHGDH and mouse anti-PSAT (B), mouse anti-PSAT and rabbit anti-PSP (C), or mouse anti-PHGDH and rabbit anti-PSP antibodies (D): Protein interaction was detected via the Duolink PLA. (E, F) Negative controls prepared by omitting the primary antibody (E), or using rabbit anti-PHGDH and mouse anti-ERAB in the primary antibody mixture (F). (G) Positive control of the PLA reaction performed using mouse anti-vimentin and rabbit anti-GFAP antibodies. Red: proximity spots indicating protein interaction. Green: cytoskeleton stained with Phalloidin CruzFluor™ 488. Blue: nuclei stained with the DraQ5 fluorescent probe. Scale bar = 15 μm. The reported images are representative of two independent experiments. (H) Density of the PLA signal expressed as the number of spots per cell as determined by manually selecting single cells in the acquired confocal stacks and using the analysis particles function of the FIJI (IMAGEJ) software. For negative and positive controls: $n = 20$; for cells labelled for PHGDH and PSAT, PSAT and PSP, and PHGDH and PSP: $n = 30$; error bars represent standard deviation.
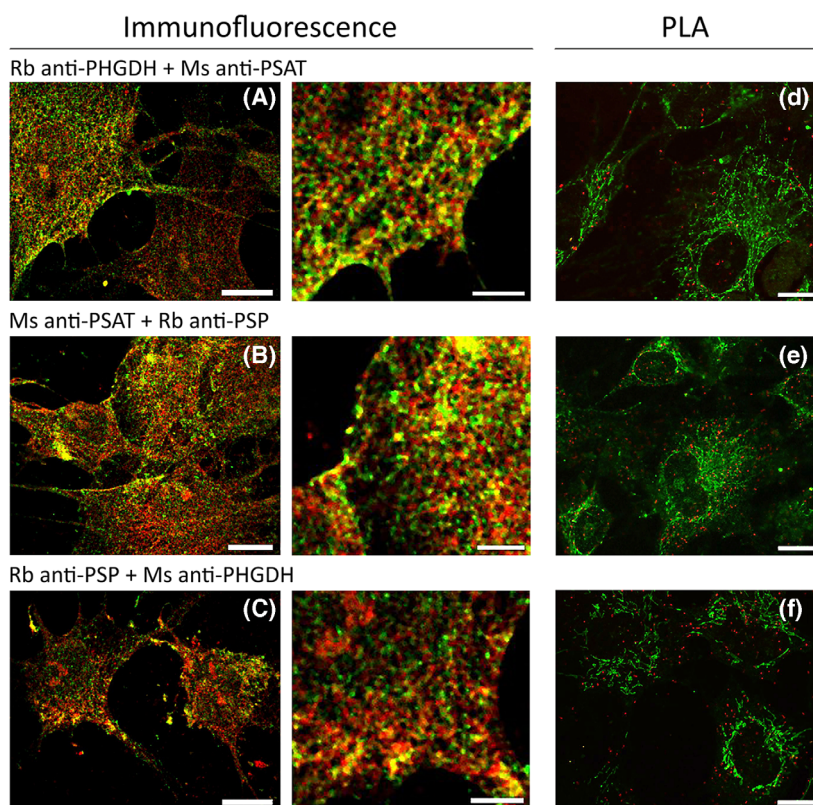
Fig. 2. Cellular distribution of the PP's enzymes in astrocytes. (A–C) Double staining immunofluorescence analyses were performed by setting up the same primary antibody mixtures used for PLA (as in Fig. 1): rabbit anti-PHGDH and mouse anti-PSAT (A); mouse anti-PSAT and rabbit anti-PSP (B), and mouse anti-PHGDH and rabbit anti-PSP antibodies (C). In green PHGDH (A) and PSP (B, C); in red PSAT (A, B) and PHGDH (C). Panels on the right represent details at higher magnification of each image. Scale bar: A–C left panels = 15 μm; right panel = 5 μm. (D–F) The cellular localisation of PP's protein complexes was investigated by detecting the three proteins in 30 DIV astrocytes using PLA. The primary antibody mixtures used in panels D–F are as in panels A–C, respectively. The localisation within the cells of the obtained proximity spots was evaluated by counter-staining the mitochondrial network with the anti-human mitochondria antibody. Red, PLA spots indicating protein interaction. Green, mitochondria. Scale bar = 15 μm. The reported images (A–F) are representative of five acquired images in the different staining conditions.

complexes. The size of these protein clusters, estimated based on the diameter of single and distinct colocalisation spots, ranged from 0.17 to 0.8 μm, with an average of 0.326 ± 0.104, 0.416 ± 0.134 and 0.376 ± 0.106 μm for PHGDH:PSAT, PSAT:PSP and PHGDH:PSP interaction, respectively. According to

[37], these clusters belong to the lower limit of the medium-size clusters (areas from 0.1 to 3 μm²).

Concerning the cellular localisation, further confocal analysis indicated that putative PP protein complexes detected by PLA do not colocalise neither with the actin network labelled with Phalloidin CruzFluor™

Table 1. Colocalisation analysis of immunofluorescence signals. The reported colocalisation coefficients were calculated by the JACoP plugin in the open-source software FIJI (IMAGEJ). Single images were processed by applying the median filter and subtracting the background (default parameters setting). Manders' coefficients were determined by adjusting the threshold of the green and red channels based on the signal detected in single cells; the automatic Costes' threshold was selected during the calculation of the Pearsons' coefficient (*r*). Values represent mean ± standard error of results from 10 to 15 imaged cells.

Immunolocalisation	Pearson's (*r*) No threshold	Pearson's (*r*) Above threshold	Manders' (M1)	Manders' (M2)
PHGDH : PSAT	0.68 ± 0.01	0.63 ± 0.02	0.58 ± 0.03	0.49 ± 0.03
PSAT : PSP	0.70 ± 0.01	0.60 ± 0.02	0.57 ± 0.03	0.51 ± 0.03
PSP : PHGDH	0.69 ± 0.02	0.62 ± 0.03	0.53 ± 0.04	0.47 ± 0.05

488 Conjugate (Fig. 1B–D) nor with the mitochondrial one stained with an anti-human mitochondria antibody (Fig. 2D–F) and appear largely distributed throughout the cytosol without apparently accumulating in a particular subcompartment, as also confirmed by immunostaining (Fig. 2).

In vitro analysis of PP complex formation

Encouraged by the results of PLA analysis, we investigated whether the three proteins are able to form a stable complex *in vitro*. The recombinant PP enzymes were separated by size exclusion chromatography (SEC) on a Superdex 200 Increase column in 50 mM Hepes, pH 7.0, 150 mM NaCl at room temperature.

The three enzymes eluted as distinct peaks: PHGDH at 12.44 ± 0.23 mL, PSAT at 16.12 ± 0.14 mL and PSP at 16.56 ± 0.04 mL. At first, the potential formation of a complex between PHGDH and PSAT was investigated after incubating the two proteins for 30 min at 4 °C, at PHGDH : PSAT molar ratios of 1 : 1, 2 : 1, 1 : 2 and 1 : 4 (the concentration of the protein at lower concentration was 16.7 μM). No evidence of a complex formation was apparent by the overlay of the resulting chromatograms (Fig. 3A–D) and by Western blot analysis of the eluted fractions. Next, under the same conditions and molar ratios, PSAT and PSP were mixed and analysed: Again, no evidence of a complex formation was apparent (Fig. 3E–H). Finally, the three enzymes were mixed
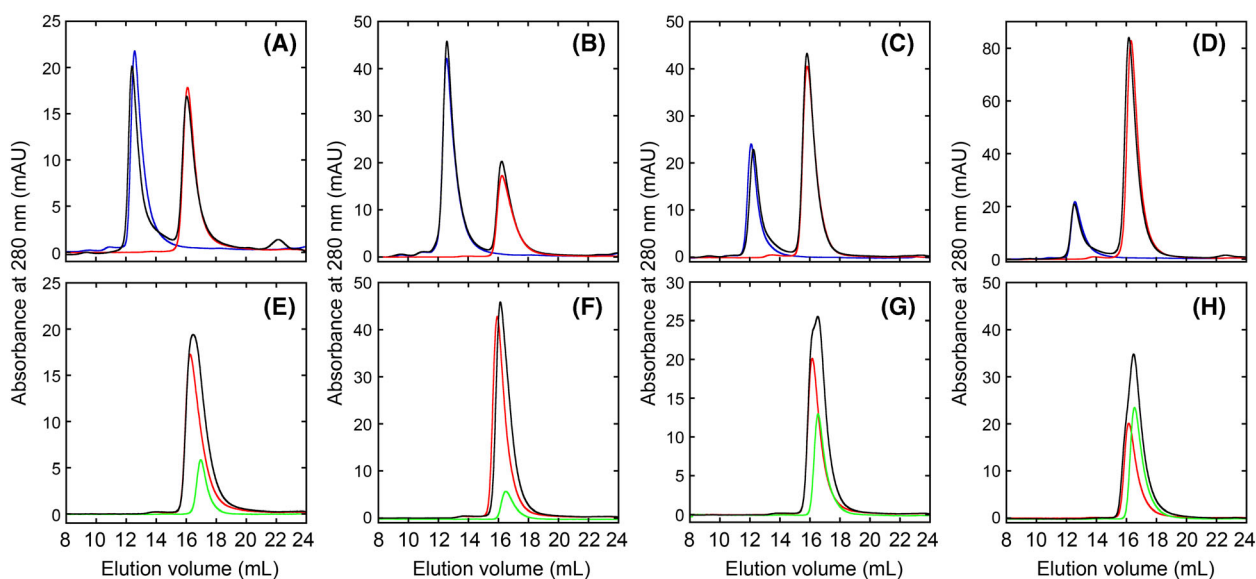
Fig. 3. Analysis of PHGDH-PSAT and PSAT-PSP complex formation by size exclusion chromatography. (A–D) SEC profiles of PHGDH and PSAT mixtures at different molar ratios: (A) 1 : 1; (B) 2 : 1; (C) 1 : 2; (D) 1 : 4. Blue line: PHGDH alone (3.35 nmol in A, C and D and 6.7 nmol in B); red line: PSAT alone (3.35 nmol in A and B, 6.7 nmol in C and 13.4 nmol in D); black line: PHGDH-PSAT mixture. (E–H) SEC profiles of PSAT and PSP mixtures at different molar ratios: (E) 1 : 1; (F) 2 : 1; (G) 1 : 2; (H) 1 : 4. Red line: PSAT alone (3.35 nmol in A, C and D and 6.7 nmol in B); green line: PSP alone (3.35 nmol in A and B, 6.7 nmol in C and 13.4 nmol in D); black line: PSAT-PSP mixture. Each SEC analysis was repeated twice.
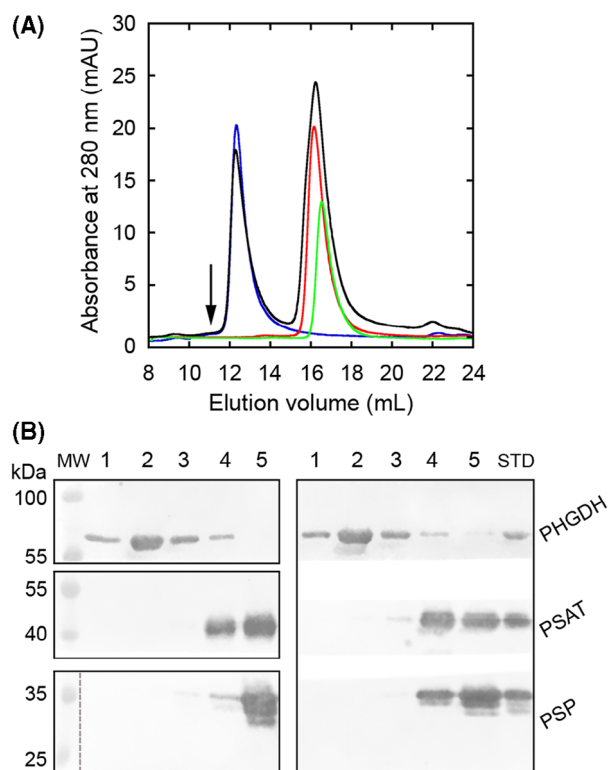
Fig. 4. Analysis of PHGDH, PSAT and PSP complex formation by size exclusion chromatography. (A) SEC profiles of PHGDH, PSAT and PSP mixture at 1 : 1 : 2 molar ratio (the theoretical elution volume of a complex made by one PHGDH tetramer, one PSAT dimer and one PSP dimer, ~ 38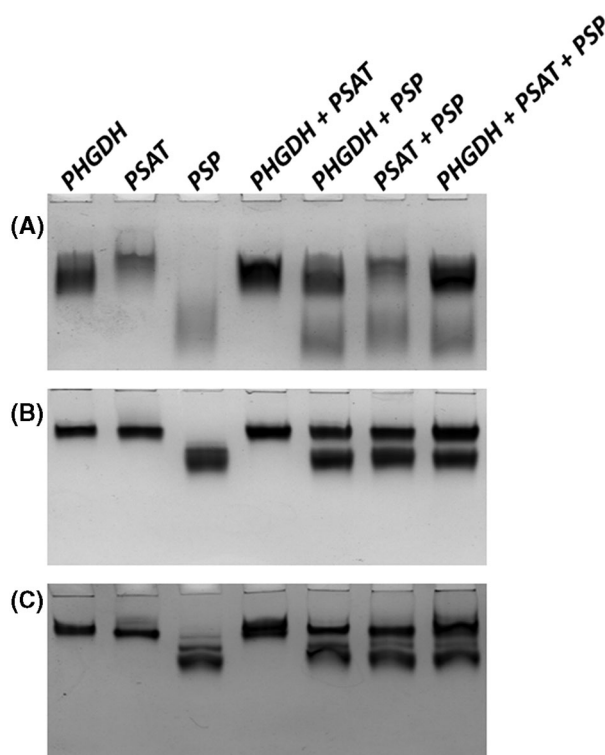0 kDa, is marked by an arrow). Blue line: PHGDH alone; red line: PSAT alone; green line: PSP alone; black line: PHGDH-PSAT-PSP mixture. SEC analysis was repeated twice. (B) Western blot analysis of the eluted fractions. MW—molecular weight markers; lanes 1–5 correspond to the eluted fractions: 1 = 10–12 mL; 2 = 12–13.5 mL; 3 = 13.5–15 mL; 4 = 15–16.5 mL; 5 = 16.5–18.5 mL; STD: 0.5 µg of the three recombinant proteins. Left: fractions collected during the elution of solutions containing the single proteins as controls (top: PHGDH alone; centre: PSAT alone; bottom: PSP alone). Right: fractions corresponding to the elution of a mixture containing 3.35 nmol of both PHGDH and PSAT, and 6.7 nmol of PSP (the membrane was cut based on protein size and incubated with the appropriate antibody). The dashed line indicates noncontinuous lanes on the same gel. The Western blot analysis was repeated twice.

Fig. 5. Native PAGE analysis of PP complex formation. (A) Native PAGE of PHGDH (77 pmol), PSAT (78 pmol) and PSP (79 pmol) at pH 9.2, 5% acrylamide. (B) Native PAGE of PHGDH (70 pmol), PSAT (96 pmol) and PSP (147 pmol) at pH 9.2, 7% acrylamide. (C) Native PAGE of PHGDH (50 pmol), PSAT (74 pmol) and PSP (110 pmol) at pH 9.2, 8% acrylamide. The native PAGE analysis was repeated twice.

together. At a PHGDH : PSAT : PSP ratio of 1 : 1 : 1 no significant change in protein distribution was observed, while at 1 : 1 : 2 ratio, an increase in PSAT and PSP relative concentration in the fraction at 15–16.5 mL was apparent (Fig. 4B, lanes 4) that should correspond to a 1 : 1 or 1 : 2 PSAT : PSP complex formation. In no cases the three proteins co-eluted in the same fraction at a lower elution volume (as demonstrated by Western blot analysis), thus excluding the formation of a stable complex under the

tested conditions. In order to evaluate whether the PP complex formation is dependent on a cell component, the SEC separations were also run following the incubation of the three enzymes with 100 µL of crude extract (corresponding to 150 µg of total protein content) from 30 DIV astrocytes for 30 min at both 4 °C and 37 °C: Again, no evidence of protein co-elution at a lower elution volume was apparent (data not shown).

The results obtained by SEC were confirmed by native PAGE performed at pH 9.2. The single proteins and the mixtures at 1 : 1 molar ratio were separated on a 5% acrylamide native PAGE (Fig. 5A): PSP showed the highest electrophoretic mobility, having a similar theoretical net charge compared with PSAT and a lower molecular mass. The mobility of PSAT and PHGDH was similar, thus hampering the unambiguous attribution of the intense band observed in the protein mixtures to the formation of a bimolecular complex (Fig. 5A). However, PSP did not participate in complex formation with any of the other two

proteins. With the aim to increase the resolution of the bands and to favour complex formation, a native PAGE on 7% acrylamide gel was performed using a molar excess of PSP and PSAT (PHGDH : PSAT : PSP = 1 : 1.5 : 2, Fig. 5B). Under these conditions, the protein bands were better resolved, but their mobility was reduced and thus the separation between PSAT and PHGDH did not improve. The increase in acrylamide concentration from 7% to 8%, while keeping all the other conditions constant, led to a further increase in resolution coupled with a decrease in protein mobility (Fig. 5C): Under these conditions, the presence of two separate bands corresponding to PHGDH and PSAT was more evident, further supporting the absence of a stable complex.

Results obtained by native PAGE and SEC were further supported by cross-linking experiments using the homobifunctional primary amine reactive cross-linker (8-atom linker) disuccinimidyl suberate (DSS). DSS was added to solutions containing the single proteins of the PP (8.35 μM for PHGDH and PSAT and 16.7 μM for PSP) at 20- or 50-fold molar excess and incubated at 4 °C for 30 min. The same procedure was used by adding DSS to a mixture containing the three enzymes at a PHGDH : PSAT : PSP molar ratio of 1 : 1 : 2. Electrophoretic and immunodetection analyses of the reaction mixtures showed that all three proteins alone generated intramolecular cross-links yielding bands at a higher apparent mass (e.g., at 30 kDa for PSP, at 90 kDa for PSAT and at > 300 kDa for PHGDH). However, no bands were specifically recognised by the three antibodies simultaneously (i.e. bands not present when the single proteins were analysed) that could correspond to links between the three enzymes, even when 2.5 mM 3PG and 0.5 mM NAD^+ or 2.5 mM 3PG, 0.5 mM NAD^+, 2.5 mM L-Glu and 3 mM $MgCl_2$ were present in the cross-linking mixture (not shown).

Kinetic analysis of the PP reaction

The kinetic parameters for the three recombinant human enzymes were determined in 50 mM Hepes, pH 7.0, at 37 °C. Since PSAT is unstable in Hepes buffer without KCl, likely as a result of aggregation, 100 mM KCl was used in the assay mixture. Similarly, PSP requires $MgCl_2$ for maximal activity [12]. On the other hand, KCl and $MgCl_2$ negatively affect PHGDH activity [31]. The kinetic parameters determined for the forward (using the hydrazine method) and reverse reactions of PHGDH were not significantly altered by the buffer composition (Table 2), thus the kinetics of the PP was also investigated in the presence of 100 mM KCl and 0.3 mM $MgCl_2$.

The reaction in the physiological direction, leading to the production of L-Ser, was investigated using the three enzymes of the PP, 3PG, NAD^+ and L-Glu, following NADH production at 340 nm in a continuous assay at pH 7 and 37 °C. The concentration of the three enzymes in the human hippocampus [22] and differentiated astrocytes (Tripodi F., Motta Z., Murtas G., Rabattoni V., Nonnis S., Grassi Scalvini F., Rinaldi A.M., Rizzi R, Bearzi C., Badone B., Sacchi

Table 2. Kinetic parameters of recombinant human PHGDH, PSAT and PSP at 37 °C and pH 7.0. In square brackets are reported the PHGDH kinetic parameters determined in presence of 100 mM KCl, 0.3 mM $MgCl_2$ and 0.1 mg·mL^{-1} BSA.

	K_{eq}	k_{cat} (s^{-1})	K_m (mM)	K_i (mM)	Reference
PHGDH					
Forward reaction[a]	0.002	2.97 ± 0.09	3PG = 0.360 ± 0.061		[31]
	[0.003]	[2.32 ± 0.05]	NAD^+ = 0.148 ± 0.021		This paper
			[3PG = 0.328 ± 0.041]		
			[NAD^+ = 0.194 ± 0.015]		
Reverse reaction		2.28 ± 0.14	3PHP = 0.010 ± 0.003	3PHP = 1.26 ± 0.25	[31]
		[1.47 ± 0.07]	NADH = 0.56 ± 0.08	[3PHP = 1.06 ± 0.29]	This paper
			[3PHP = 0.015 ± 0.03]		
			[NADH = 0.66 ± 0.14]		
PSAT					
Forward reaction	10	23.8 ± 1.1	3PHP = 0.004 ± 0.002	3PHP = 0.23 ± 0.14	[33]
			L-Glu = 2.4 ± 0.4	L-Glu = 7.1 ± 3.9	
Reverse reaction		8.6 ± 0.2	α-KG = 0.36 ± 0.04	α-KG = 8.4 ± 4.7	[33]
			3PS = 0.033 ± 0.005	3PS = 3.4 ± 2.0	
PSP	Irreversible	44.8 ± 0.9	3PS = 0.040 ± 0.003	L-Ser = 0.5 mM	[32,39]

[a]Using the hydrazine assay.

Table 3. Concentration of the enzymes and main metabolites related to the phosphorylated pathway.

Enzymes	Concentration	
	Differentiated astrocytes[a] (ng·µg⁻¹ protein, [µM])	Human hippocampus[b] (ng·µg⁻¹ protein)
PHGDH	1.4 [0.82]	0.41 ± 0.22
PSAT	1.2 [1.14]	1.11 ± 0.25
PSP	0.1 [0.12]	0.019 ± 0.009
PHGDH : PSAT : PSP		
Amount ratio	14 : 12 : 1	20 : 55 : 1
Molar ratio	7 : 8 : 1	10 : 26 : 1

Metabolites	Concentration (µM)	Localisation	Reference
3PG	45	Red blood cells (cytosolic)	[53]
	110–180	Breast cancer cells	[41]
3PHP	Below detection	Breast cancer cells	[41]
NAD⁺	88.7	Cytoplasm	[53]
	300	Brain tissue	[54]
	770–990	Breast cancer cells	[41]
NADH	60	Brain tissues	[54]
	190–370	Breast cancer cells	[41]
ʟ-Glu	1400 ± 200	Hybridoma cell line (cytosolic)	[55]
α-KG	320	Hybridoma cell line (cytosolic)	[55]
	470–550	Breast cancer cells	[41]
3PS	5	CSF	[56]
ʟ-Ser	1180 ± 490	Human hippocampus	[22]
	1020 ± 260	Differentiated astrocytes	a
ᴅ-Ser	55.82 ± 23.46	Human hippocampus	[22]
	7.72 ± 3.09	Differentiated astrocytes	a
Gly	1910 ± 620	Human hippocampus	[22]
	6790 ± 3610	Differentiated astrocytes	a

[a]Tripodi F., Motta Z., Murtas G., Rabattoni V., Nonnis S., Grassi Scalvini F., Rinaldi A.M., Rizzi R, Bearzi C., Badone B., Sacchi S., Tedeschi G., Maffioli E., Coccetti P., Pollegioni L, unpublished data *F., Motta Z., Murtas G., Rabattoni V., Nonni.*; [b]Ref. [22].

S., Tedeschi G., Maffioli E., Coccetti P., Pollegioni L, unpublished data) was recently determined, as well as the concentration of the main metabolites related to the PP (Table 3). In order to simulate the physiological conditions, the reactions were performed using the concentration of the PP enzymes as determined in differentiated astrocytes, i.e. 0.82 µM PHGDH, 1.14 µM PSAT and 0.12 µM PSP (Table 3). The increase in the concentration of 3PG from 0.053 mM (i.e. the physiological concentration) to 2.53 mM, keeping the concentration of NAD⁺ and ʟ-Glu around the physiological values (0.3 and 2 mM, respectively), led to a proportional increase in the reaction rate (Fig. 6A). Consistently, when the same reaction was followed by monitoring phosphate produced by the last enzyme, the time course overlapped well with the reaction monitored through the production of NADH (Fig. 6E). The reactions at fixed 0.53 mM 3PG and 2 mM ʟ-Glu concentrations showed a significant increase in reaction rate upon increasing NAD⁺ concentration (Fig. 6B), while a modest increase in the reaction rate was observed when raising the concentration of ʟ-Glu

from 0.2 to 2 mM, with no additional effects at 20 mM ʟ-Glu (Fig. 6C). Instead, at the low, physiological concentration of 3PG (i.e. 0.053 mM), the effect of increasing ʟ-Glu concentration was negligible (Fig. 6D). Since the K_m of PSAT for ʟ-Glu is 2.4 mM, the rate of PSAT reaction limits the flux at high 3PG and low ʟ-Glu concentrations (Fig. 6C). The effect of enzyme concentrations on the flux through the pathway was assessed by varying the concentration of one enzyme around its physiological value while keeping the concentration of the others constant (Fig. 7). Differently from what is reported in the literature for the PP from rabbit liver [38] and under the conditions tested, PSP did not affect the rate of the flux through the PP (Fig. 7C). Quite unexpectedly, at a physiological 1 mM ʟ-Ser concentration the rate of phosphate production by the PP did not decrease significantly, this indicating that the final product apparently does not modulate the flux through the pathway (Fig. 6F). The reason of this behaviour is apparent when the reduction in free PSP concentration at 1 mM ʟ-Ser is taken into account. Considering a K_i of 0.5 mM and a
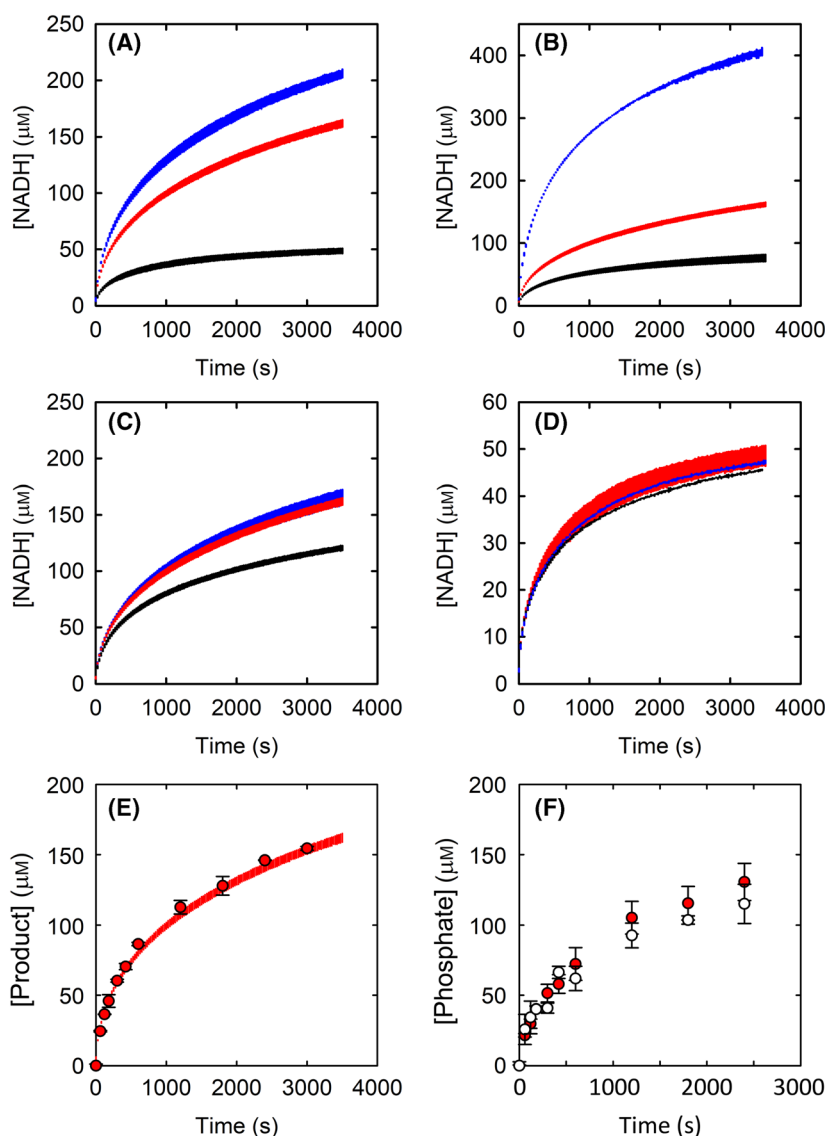
Fig. 6. Kinetics of the PP followed as NADH and phosphate production. The reactions were carried out in 50 mM Hepes, 100 mM KCl, 0.3 mM MgCl$_2$, 0.1 mg·mL^{-1} BSA, pH 7, 37 °C. The enzyme concentrations were as follows: 820 nM PHGDH, 1140 nM PSAT and 120 nM PSP. The substrates were used at the following concentrations: 2 mM L-Glu, 0.3 mM NAD$^+$ and 0.54 mM 3PG. Panels (A–D) The concentration of one substrate at a time was changed as follows: (A) 3PG concentration: 0.054 (black), 0.54 (red) and 2.53 mM (blue); (B) NAD$^+$ concentration: 0.09 (black), 0.3 (red) and 3 mM (blue); (C, D) L-Glu concentration: 0.2 (black), 2 (red) and 30 mM (blue). In panel D, L-Glu concentration was as in panel C, while 3PG concentration was set at the physiological value of 0.053 mM. Bars are the average ± SD of two replicates. (E) Overlay of the kinetic traces of the overall reaction catalysed by the enzymes of the PP as monitored by either the absorbance at 340 nm of NADH (red bars) and the phosphate production evaluated by the malachite green assay (red dots). (F) Overlay of the kinetic traces collected in the same conditions as those used in panel E either in the absence (red dots) or in the presence (white dots) of 1 mM L-Ser

noncompetitive inhibition mechanism, see Table 2 and Ref. [39], at 1 mM L-Ser, about 67% of PSP should be complexed with L-Ser; thus, the concentration of free, active enzyme should decrease from 120 to 40 nM: This reduction is comparable to the one reported in Fig. 7C that did not affect the overall rate.

The experimental traces for NADH and phosphate production (the latter corresponding to L-Ser production) were determined at 50 mM Hepes, pH 7.0 and 37 °C using 0.82 μM PHGDH, 1.14 μM PSAT and 0.12 μM PSP (corresponding to theoretical rates v_f and v_r of 0.0025 and 0.0019 mmol·L^{-1}·s^{-1} for
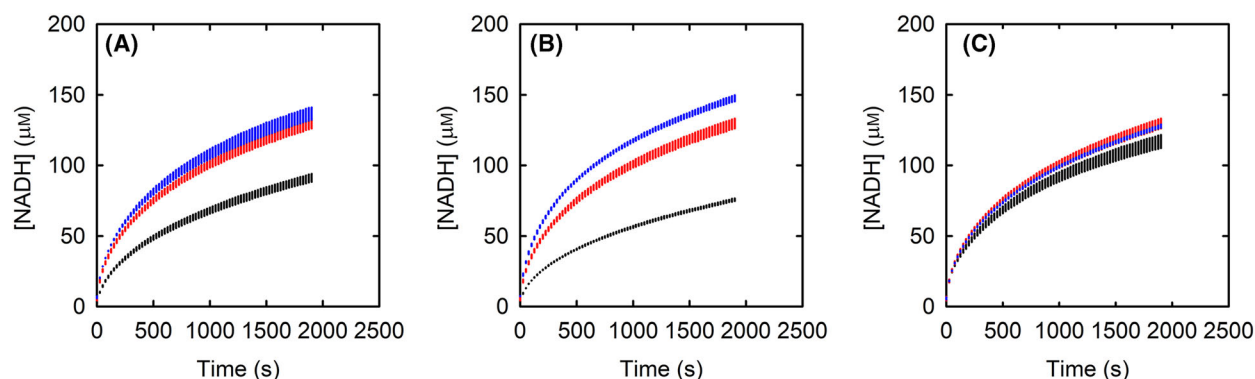
Fig. 7. Effect of the relative concentration of each enzyme on the kinetics of the PP. (A) Effect of PHGDH concentration: 200 nM (black), 820 nM (red) and 1600 nM (blue). (B) Effect of PSAT concentration: 200 nM (black), 1140 nM (red) and 4700 nM (blue). (C) Effect of PSP concentration: 20 nM (black), 120 nM (red) and 600 nM (blue). Conditions: 50 mM Hepes, pH 7.0, 100 mM KCl, 0.3 mM MgCl₂, 0.1 mg·mL⁻¹ BSA, 2 mM L-Glu, 0.3 mM NAD⁺ and 0.54 mM 3PG, 37 °C. Bars are the mean ± SD of two replicates.
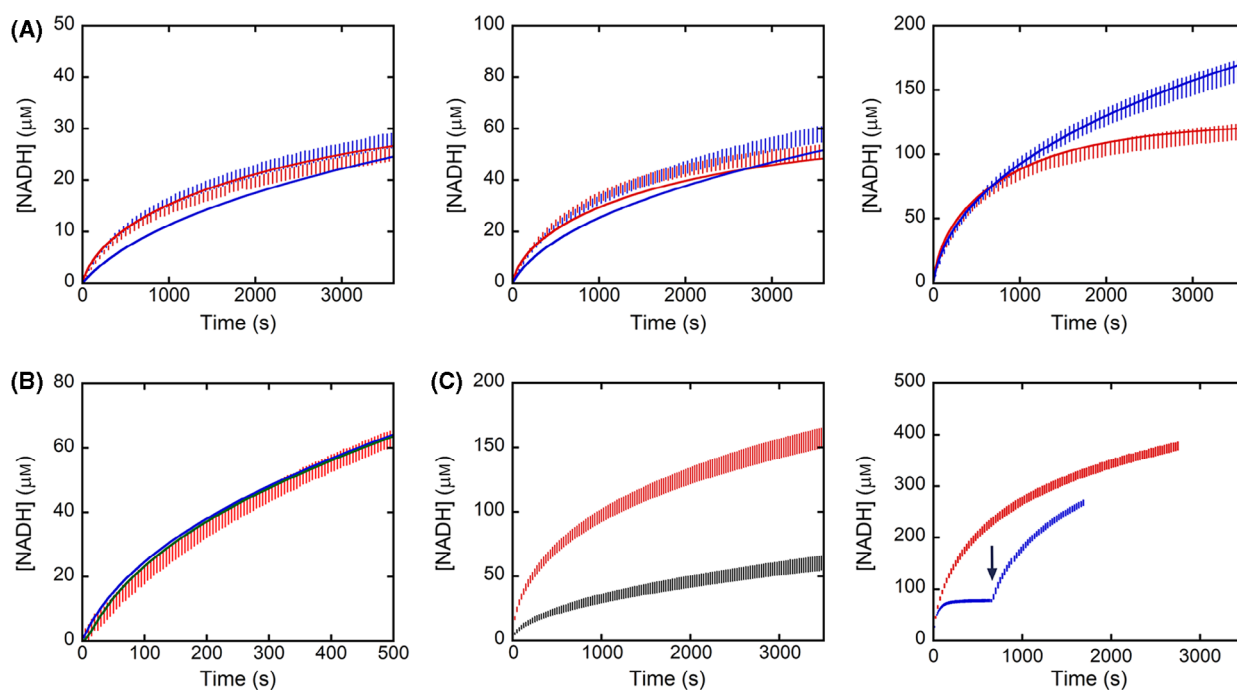
Fig. 8. Simulation of NADH formation during the reaction of the enzymes of the PP. (A) Comparison of experimental traces (average of 3 measurements ± SD) with (blue bars) and without PSP (red bars) and simulation traces (lines). Conditions: 820 nM PHGDH, 1140 nM PSAT, 120 nM PSP, 0.54 mM 3PG, 2 mM L-Glu and 0.09 mM (left), 0.3 mM (centre) or 3 mM (right) NAD⁺ (37 °C and pH 7.0). (B) Close-up of the reaction reported in panel A right at short times. In blue the simulation for NADH production; in green the simulation for L-Ser production; and in red bars the experimental trace. (C) Effect of added salts on the overall reaction catalysed by the enzymes of the PP. Left: the reaction, carried out at 37 °C, contained 820 nM PHGDH, 1140 nM PSAT, 120 nM PSP, 2 mM L-Glu, 0.3 mM NAD⁺ and 0.54 mM 3PG in either 25 mM Hepes pH 7.0 (black) or 50 mM Hepes, pH 7.0, 100 mM KCl, 0.3 mM MgCl₂, 0.1 mg·mL⁻¹ BSA (red). Bars are the mean ± SD of two replicates. Right: PSP drives the PP towards L-Ser synthesis: comparison of the trace for NADH production when PSP was present from the beginning (red) with the one recorded adding PSP when NADH level reached a plateau (blue). Conditions as in the left panel with the exception of NAD⁺ concentration, which is 3 mM. Bars represent the average ± SD of two replicates.

PHGDH, of 0.027 and 0.0097 mmol·L⁻¹·s⁻¹ for PSAT and of 0.00538 mmol·L⁻¹·s⁻¹ for PSP), were simulated by the COPASI software (http://www.copasi.

org). For each condition, the traces with and without PSP were evaluated (Fig. 8A): The NADH concentration time courses did not show any lag, were faster

than expected based on the known kinetic parameters and were further pushed in the direction of L-Ser production by PSP. At first, we observed that a reasonable simulation was obtained only when the forward rate v_f for PHGDH was 50-fold higher (0. 125 mmol·L^{-1}·s^{-1}) than that based on the kinetic parameters determined in Ref. [31] and the K_m for NAD$^+$ was 75 vs 150 μM. While the latter change is of small amplitude (2-fold), the rate of 3PHP production by PHGDH is significantly different between the simulation and the published values. The explanation is provided by recent work [40] demonstrating that the oligomerisation state and the apparent k_{cat} of PHGDH are both altered by the enzyme concentration: The homotetrameric state and the maximal figure of k_{cat} are observed at ≥ 1 μM enzyme concentration. Actually, the PHGDH kinetic parameters have been previously determined at 0.007 μM enzyme concentration [31], while present investigations were performed at 0.82 μM. The change in v_f as suggested by the simulation studies agrees with that reported for enzyme activity in fig. 6 in Ref. [40].

Next, experimental traces and simulations of NADH and L-Ser production demonstrated that the former is produced slightly faster at the beginning of the reaction while the concentrations of both products are very close at times ≥ 500 s (Fig. 8B): When NADH is produced upon reduction of 3PG, the intermediate 3PHP is quickly converted into the L-Ser final product by the PSAT and PSP reactions. Under these conditions, PHGDH seems to be rate limiting since its rate strongly depends on 3PG level (i.e. from glycolysis) and NAD$^+$/NADH ratio (i.e. from redox balance). Finally, when the reaction was carried out in the presence of 100 mM KCl, 0.3 mM MgCl$_2$ and 0.1 mg·mL^{-1} bovine serum albumin (BSA) a significant increase in NADH production was observed (Fig. 8C, left): The simulation suggests an increase in K_{eq} value for PHGDH (from 0.00002 to 0.0005–0.001, thus reaching a value close to the one determined under static conditions, i.e. 0.002, see Table 2). The effect of PSP in pushing the PP in the direction of L-Ser production was further evident under these experimental conditions (Fig. 8C, right).

In conclusion, the kinetic analyses demonstrate that the three enzymes of the PP work together and seem well coupled under *in vitro* conditions since the overall time course of product formation is well simulated using the kinetic parameters determined for every single enzyme, with no evidence of lag times in product formation and of slowdown due to products diffusion, i.e. the three enzymes work as a putative metabolic cluster.

The production of the oncometabolite 2-hydroxyglutarate

The ability of PHGDH from *Escherichia coli* to use α-ketoglutarate (α-KG) as a substrate with reoxidation of NADH (in the reverse direction) was reported by [17], a pathway in which synthesis proceeds efficiently without a net consumption of NAD$^+$. In tumour cells, this cycle generates the oncometabolite 2-hydroxyglutarate, whose accumulation in breast cancer cells is associated with poor diagnosis. The ability of human PHGDH to use α-KG in the reverse direction was previously reported [31,41]. Here, we evaluated the ability of the human PP to generate a cycle in which NADH generated by PHGDH in the forward direction is recycled into NAD$^+$ by using α-KG, with the simultaneous production of phosphate and 2-hydroxyglutarate. As shown in Fig. 9, when a low NAD$^+$ concentration was used (30 μM), no difference in phosphate production with or without 0.4 mM α-KG was evident. Under these conditions, NAD$^+$ is the limiting reagent and a final concentration of phosphate of about 30 μM is obtained, indicating that once this reagent is depleted it cannot be recycled by the reverse PHGDH reaction. However, the concentration of NADH produced under these conditions might be too low compared with the K_m of PHGDH (about 0.5 mM, Table 2). Anyway, when the experiment was carried out at 0.3 or 3 mM NAD$^+$ in either the absence or presence of 0.4 mM α-KG, again no effect of the latter on the progress of the reaction was apparent. This excluded that the human PP generates the oncometabolite under these conditions.

Discussion

The *de novo* L-Ser biosynthesis pathway relies on three enzymes to catalyse the conversion of the glycolytic intermediate 3PG into L-Ser (Scheme 1). PLA analyses on differentiated human astrocytes demonstrated that the three enzymes are in close proximity (< 40 nm) in the cytosol, suggesting a closer proximity between PSAT and PSP compared with the PHGDH-containing complex. This is also confirmed by confocal analysis, showing a lower degree of colocalisation between PHGDH and PSAT and thus suggesting the existence of an equilibrium between free and complexed PHGDH enzyme forms in the cytosol. An overall figure of 47–58% of total PHGDH, PSAT and PSP proteins colocalise in the cytoplasm of differentiated astrocytes, generating clusters with a diameter of 0.33–0.42 μm (a putative serinosome), similar to the one reported for the purinosome in HeLa and LND cells
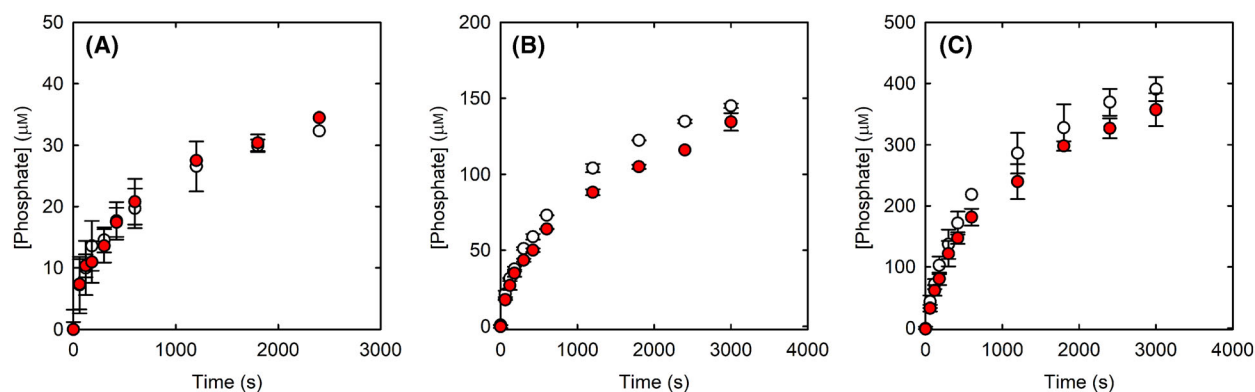
Fig. 9. Assessment of NAD$^+$ recycling by the enzymes of the PP. Phosphate produced over time by the *in vitro* reconstructed PP was measured using the malachite green assay in the presence (red symbols) and absence (white symbols) of 0.4 mM α-KG and different concentrations of NAD$^+$ (0.03 mM, panel A; 0.3 mM, panel B; 3 mM panel C) at 37 °C. The concentration of the other reagents is kept constant (820 nM PHGDH, 1140 nM PSAT, 120 nM PSP, 50 mM Hepes pH 7.0, 100 mM KCl, 0.54 mM 3PG, 0.3 mM MgCl$_2$, 2 mM L-Glu). Bars are the mean ± SD of two replicates.

[42]. The 200–300 nm in diameter size of the functional purinosome should contain a total of 10^3 to 10^5 enzyme molecules.

In vitro studies using recombinant PHGDH, PSAT and PSP failed in generating a stable (detectable and separable) complex made by the three enzymes of the PP. The results of SEC, native PAGE and chemical cross-link experiments agree and indicate that neither a bimolecular complex nor a trimolecular one forms at the protein concentrations used (up to 66.9 μM). This is not unusual, considering that several attempts to purify and reconstitute *in vitro* metabolic complexes failed, due to the highly dynamic and weak interactions that hold these enzymes together [43]. Up to now, the physical interactions were reported only for PHGDH and PSAT from *Entamoeba histolytica*, an enteric human parasite: The protein–protein complex exhibited a 1 : 1 stoichiometry and a dissociation constant of 0.35 μM [44]. Our results do not exclude that the interaction between the three enzymes of the PP could be modulated by additional cellular components or by post-translational modifications related to specific cell signals. Indeed, metabolons are known to be often associated with structural elements of the cell (e.g. membranes and cytoskeleton) and nonenzymatic proteins, which act not only as scaffolding elements to stabilise them but also play a role in the modulation of these functional agglomerates [45]. Anyway, kinetic experiments suggest the proximity of the PP human enzymes: The enzymes of the PP are kinetically coupled under *in vitro* conditions, with no evidence of lag times in product generation and of reaction slow-down due to product diffusion: They behave as a putative metabolic complex (a metabolon assembly). By using enzyme concentrations corresponding to those identified *in vivo*, PHGDH seems the rate-limiting step of the PP (PSAT could be rate limiting at low glutamate concentrations and high, nonphysiological, 3PG concentrations) and PSP the driving force to generate L-Ser thus bypassing the reversibility of the two previous steps. This observation agrees with the larger number of pathological variants reported for PHGDH and PSAT compared with PSP [5]. The product L-Ser, a noncompetitive inhibitor of PSP, does not affect the overall reaction at 1 mM concentration (i.e. the physiological value), as expected considering that this enzyme, under the conditions tested here, does not limit the flux through the pathway.

Once, cells were considered to consist of a collection of soluble proteins, substrates, cofactors and products within the cellular matrix that relied primarily on diffusion for the right components to come together and react. With the advancements in the understanding of cellular organisation, compartmentalisation, membrane-bound systems and formation of multimolecular complexes were discovered as suitable strategies used by cells to organise and control the enzymes of particular pathways [46,47]. This study establishes that the three enzymes involved in the important biosynthesis of L-Ser in human cells are functionally connected through the formation of a protein agglomerate (a serinosome). Dynamic assemblies of enzymes for efficient and regulated metabolism have been previously observed in purine metabolism [29,42]. The PP metabolon assembly generated by transient interactions of the three enzymes provides a channelling solution for the pathway intermediates, giving higher local concentration and efficient processing of intermediates,

preventing their bulk equilibration with the cytosol thus increasing the pathway flux and definitely pushing the process to L-Ser production. Optimal distribution of enzymes in a large cell given by multiple enzyme clusters is 110-fold more efficient than a delocalised distribution for a three-step pathway [27].

The observed aggregates might represent a partial assembly of the PP enzymes that should undergo further co-clustering in response to varying metabolic demands. This enzyme agglomerate assembly delivers a relevant level of sophistication to the control of L-Ser biosynthesis in human cells (especially in CNS where L-Ser is used to produce the *N*-methyl-D-aspartate receptor coagonist D-Ser) and implies the need to shed light on various structural details. In particular, on the post-translational modifications of each enzyme (selected phosphorylation of PHGDH has been reported to mediate its nuclear targeting under glucose deprivation in cancer cells) [48], the significance of PHGDH allosteric machinery for the integration of the metabolic signals that modulate the PP and the specific signals controlling the cluster assembly and disassembly.

Materials and methods

Protein expression and purification

Recombinant human His-PHGDH (herein named PHGDH) was expressed in *E. coli* and purified as reported in Ref. [31]. The final enzyme preparation was stored in 50 mM Hepes, pH 7 and 5% glycerol (v/v). PHGDH concentration was determined based on the extinction coefficient at 280 nm (40 450 $M^{-1} \cdot cm^{-1}$). Recombinant His-tagged human PSAT was expressed and purified following a published procedure [33]. PSAT was purified from the crude extract by IMAC (Talon Superflow—Cytiva™). Purified PSAT was then dialyzed against 25 mM Tris pH 6.8, 300 mM NaCl, 1 mM TCEP and 4 μM pyridoxal-5′-phosphate to remove imidazole. Finally, PSAT was concentrated, flash-frozen in liquid nitrogen and stored at −80 °C. Recombinant His-tagged human PSP was expressed in *E. coli* cells and purified following a published procedure [32]. The protein was purified from the cell extract on Talon Superflow resin (Cytiva™, Marlborough, MA, USA) and stored in 25 mM Hepes, 100 mM NaCl, pH 7.4, at −80 °C. The concentrations of human PSP and PSAT were estimated using the extinction coefficients at 280 nm of 11 460 and 35 870 $M^{-1} \cdot cm^{-1}$, respectively, calculated by Protparam (Expasy, http://www.expasy.org). Recombinant PHGDH, PSAT and PSP possess a molecular mass of 59.77, 42.85 and 27.17 kDa, respectively.

Concerning standard assay, PHGDH-specific activity in the physiological direction was determined by monitoring NADH fluorescence intensity (recording the emission at 450 nm following excitation at 360 nm) over time at 37 °C in 96-well plates with TECAN Infinite 200 Pro reader (Männedorf, Switzerland). The assays were performed using 0.04 μg PHGDH in 25 mM Hepes, pH 7.0, 2.5 mM 3PG and in the presence of 1.5 mM NAD$^+$ and 200 mM hydrazine or 1.7 μM PSAT in the presence of 30 mM L-Glu (100 μL total volume; hydrazine and PSAT are required to drive the reaction forward). The activity in the reverse direction was determined by monitoring the decrease in NADH fluorescence intensity over time at 37 °C. The assays were performed using 0.6 μg of enzyme in 25 mM Hepes, pH 7.0, using different amounts of PHP and 5 mM NADH or of 0.5 mM PHP and different amounts of the cofactor.

The catalytic parameters of PSAT (Table 2) were determined at 37 °C for the forward direction by a coupled assay using glutamate dehydrogenase (GDH) as the coupling enzyme in a buffer solution containing 50 mM Hepes pH 7.0, 100 mM KCl, 1 mM dithiothreitol, 0.170 mM pyridoxal-5′-phosphate. The assay mixture contained 81 nM PSAT, 1 U GDH, 0.1 mM NADH, 32 mM NH₄Cl, 0.011–0.11 mM 3PHP and 0.4–80 mM L-Glu. The activity in the reverse direction was measured by a continuous assay coupled with PHGDH in the same buffer used for the forward direction. The assay mixture contained 337 nM PSAT, 8 mU PHGDH, 0.1 mM NADH, 0.1–10 mM α-KG and 0.03–1 mM 3PS.

The catalytic parameters of PSP (Table 2) were determined at 37 °C by a published continuous method detecting the released serine by the coupled enzyme *Haemophilus influenzae* serine acetyltransferase (HiSAT) [32]. In detail, the assay was performed in a buffer solution containing 50 mM Hepes pH 7, 100 mM KCl and 3 mM MgCl₂. The assay mixture contained 0.17 mM acetyl-CoA, 0.5 mM DTNB, 430 mU HiSAT and 0.010–0.5 mM 3PS.

Native PAGE

The pI of PHGDH, PSAT and PSP (6.356, 7.634 and 6.342, respectively) and their net theoretical charge at a given pH were calculated using the Protein Tool in Prot Pi bioinformatic toolbox (https://www.protpi.ch/) and correspond, respectively, to: 3.617, 9.695 and 2.620 at pH 6.0; −10.702, −1.767 and −6.083 at pH 8.0; −23.951, −13.082 and −11.226 at pH 9.2. Native PAGE was performed on a continuous gel system with 5–8% acrylamide in 50 mM Tris, 25 mM boric acid, pH 9.2. The protein samples were mixed, incubated at room temperature for 5 min, added to a nondenaturing sample buffer (running buffer with the addition of 10% glycerol and 0.2 mg·mL^{-1} bromophenol blue) and loaded on the gel. The electrophoretic run was performed in the cold room at a constant voltage of 200 V.

Size exclusion chromatography

The evaluation of PHGDH, PSAT and PSP complex formation was performed by SEC using a Superdex 200 Increase (Cytiva^{TM}) column using an Akta chromatography system (Cytiva^{TM}) at room temperature in 50 mM Hepes pH 7.0, 150 mM NaCl, at a flow rate of 0.5 mL·min^{-1}. Sample mixtures were prepared by mixing different molar amounts of the three proteins diluted in the elution buffer, incubated at 4 °C for 30 min and centrifuged before column injection. Single proteins were also analysed as a control. SEC separations were also performed after the incubation of the three enzymes of the PP with 100 μL of crude extract from 30 DIV astrocytes for 30 min at both 4 °C or 37 °C. Briefly, the cell pellet was suspended in ice-cold lysis buffer (50 mM Hepes pH 7.0, 0.7 μg·mL^{-1} pepstatin, 1 μg·mL^{-1} leupeptin, 1 mg·mL^{-1} DNAse) and sonicated. Cell lysate was then centrifuged at 13 000 *g* for 30 min at 4 °C; the protein concentration of the supernatant was quantified using the Bradford reagent (Merck, Rahway, NJ, USA). The formation of a complex was verified by observing the appearance of new peaks, by evaluating peak areas and by SDS/PAGE and western blot analyses of eluted fractions. For western blot analysis, the membranes were blocked overnight at 4 °C with 4% dried milk in Tris-buffered saline (TBS; 10 mM Tris–HCl pH 8.0, 0.5 M NaCl) with the addition of 0.1% Tween-20 (TBST) and subsequently incubated with primary antibodies diluted in 2% dried milk in TBST for 2 h at room temperature. After extensive washing, the membranes were incubated for 1 h at room temperature with goat anti-rabbit IgG Alexa Fluor plus 800 (1 : 20 000; Invitrogen). The fluorescent signals were detected using the Odyssey Fc Imaging System (LI-COR Biosciences, Lincoln, NE, USA). The primary antibodies used were as follows: rabbit polyclonal anti-PHGDH (1 : 1000; Invitrogen); rabbit polyclonal anti-PSAT (1 : 1000; Antibodies-online, Aachen, Germany); rabbit polyclonal anti-PSP (1 : 2000; Thermo Fisher Scientific, Waltham, MA, USA).

Cross-linking

PHGDH, PSAT and PSP were mixed (at 1 : 1 : 2 molar ratio), incubated at 4 °C for 30 min in 50 mM Hepes, pH 7.0, 150 mM NaCl and then cross-linked with a 20 or 50-fold molar excess of DSS (with respect to PHGDH monomer) for 30 min at 25 °C; the reaction was stopped by adding Tris–HCl, pH 8.0 to a final concentration of 20 mM. The formation of a complex was evaluated by 8% SDS/PAGE and western blot analyses.

The PP kinetics

While every single enzyme is usually assayed under slightly different conditions (see above), the overall reaction was measured in 50 mM Hepes buffer, pH 7.0 and at 37 °C.

For PSAT and PSP, the presence of 0.1 mg·mL^{-1} albumin from bovine serum (BSA), 100 mM potassium chloride and 0.3 mM magnesium chloride is required for optimal activity [49], while both these salts negatively affect the activity of PHGDH [31]. Therefore, assays were carried out both with and without the chloride salts. The reaction mixture that contains PHGDH, PSAT, PSP, NAD$^+$ and L-Glu was incubated at 37 °C for 5 min and the reaction was initiated by adding 3PG. The progression of the reaction was followed by two methods: the continuous spectroscopic detection of NADH production by PHGDH and the determination of the phosphate release in the final step of the pathway using the malachite green assay [32]. NADH formation was followed either by its absorption at 340 nm or by its fluorescence emission at 450 nm upon excitation at 340 nm: These two detection methods were comparable. The determination of the phosphate release was performed on 20 μL aliquots of the reaction mixture sampled over time and mixed with 2 μL 10% trichloroacetic acid to stop the reaction. 100 μL of malachite green reagent (MAK308; Merck) were added to the solution and the absorbance at 620 nm was recorded using a HALO LED 96 microplate reader (Dynamica, Livingstone, UK) after 30 min incubation at room temperature in the dark.

The simulation of the kinetics for the PP in terms of NADH and phosphate production was carried out using COPASI 4.37 software (http://www.copasi.org). The reaction of PHGDH was set up as a bi-bi reversible reaction with an equilibrium constant ≤ 0.002; the reaction of PSAT was set up as a ping-pong reaction with an equilibrium constant of 10–40; the reaction of PSP was set up as a Henri–Michaelis–Menten irreversible reaction; the kinetic constants reported in Table 1 were used for the simulations.

In situ PLA and immunofluorescence analyses

Induced pluripotent stem cells-derived astrocytes at 30 DIV, kindly provided by P. Coccetti's lab (Department of Biotechnology and Biosciences, University of Milano-Bicocca, Milan, Italy) and showing a signature of molecular markers similar to mature astrocytes rather than to reactive ones (Tripodi F., Motta Z., Murtas G., Rabattoni V., Nonnis S., Grassi Scalvini F., Rinaldi A.M., Rizzi R, Bearzi C., Badone B., Sacchi S., Tedeschi G., Maffioli E., Coccetti P., Pollegioni L, unpublished data), were seeded on matrigel-coated coverslips (4×10^4 cells each), fixed in ice-cold 4% paraformaldehyde for 15 min and permeabilised with 0.2% Triton X-100 in PBS for 20 min at room temperature. Cells were then subjected to PLA using the Duolink *In Situ* Orange starter kit mouse/rabbit (DUO92008; Merck) according to the manufacturer's protocol. This assay is based on the work by Fredriksson *et al.* [50] who set up a highly specific and sensitive method for protein detection relying on the complementation of two DNA aptamer probes with sequence extensions that could

be joined by ligation. In this way, probes that bind in close proximity by recognising the same target molecule could be joined to form a template for detection via sensitive real-time PCR amplification. In subsequent works, aptamers were replaced by oligonucleotide-conjugated antibodies, serving as proximity probes and PLA was applied for detecting protein–protein interaction in fixed cells or tissues. Briefly, after permeation in PBS, 0.2% Triton X-100 (20 min at room temperature), coverslips were incubated in Duolink blocking solution for 60 min at 37 °C and then with primary antibodies overnight at 4 °C. Different primary polyclonal antibody mixtures were prepared in Duolink antibody diluent as follows: (a) rabbit anti-PHGDH (1 : 1000, HPA024031; Sigma) + mouse anti-PSAT (1 : 250, H00029968-A01; Abnova, Taipei, Taiwan); (b) mouse anti-PSAT (1 : 250) + rabbit anti-PSP (1 : 250, PA5-22003; Invitrogen); (c) mouse anti-PHGDH (1 : 500, raised against the purified recombinant protein; Davids Biotechnologie, Regensburg, Germany) + rabbit anti-PSP (1 : 250). Coverslips were then incubated with PLA Probe MINUS and PLUS for 1 h at 37 °C, with the ligation solution for 30 min at 37 °C and finally with the amplification solution for 100 min at 37 °C. After each incubation, an extensive washing in Duolink buffer A was performed. Next, the cells were rinsed with Duolink buffer B and counterstained with Phalloidin CruzFluor™ 488 Conjugate (1 : 1000, sc-363791; Santa Cruz Biotechnology, Dallas, Texas, USA) for 60 min at room temperature to visualise the cytoskeleton or with the Ms X Hu Mitochondria mouse monoclonal antibody (1 : 1000, MAB1273; Millipore, Burlington, MA, USA; overnight at 4 °C) and the Alexa Fluor 488 donkey anti-mouse antibody (1 : 100, A21202; Invitrogen; 60 min at room temperature), and with the fluorescent nuclear probe DraQ5 (1 : 500, 62251; Thermo Fisher Scientific) for 10 min at room temperature. Finally, coverslips were mounted with a Vectashield mounting medium (H-1000-10; Vector Laboratories, Zurich, Switzerland). Negative controls were prepared by omitting primary antibodies; or by using a mixture containing rabbit anti-PHGDH (1 : 1000) and mouse monoclonal anti-ERAB (1 : 500, sc-136326; Santa Cruz Biotechnology) antibodies. ERAB is a 27 kDa protein known to localise to the endoplasmic reticulum and the mitochondrial matrix [51], which therefore cannot interact with the cytosolic PHGDH. On the other hand, a primary antibody mixture containing rabbit polyclonal anti-GFAP (1 : 2000, Z0334; Dako, Santa Clara, CA, USA) and mouse monoclonal anti-vimentin (1 : 200, M0725; Dako) was used as a positive control for the Duolink reaction, since these type III intermediate filament proteins expressed in astrocytes are known as co-polymerisation partners [52]. The number of PLA spots/cell was determined by selecting ROI corresponding to single cells and using the analysis particles function of the open-source software FIJI (IMAGEJ; https://imagej.net/software/fiji)

after having properly adjusted the colour threshold of images.

Immunofluorescence analyses on iPSC-derived astrocytes at 30 days were performed by double staining using the same primary antibodies and the same dilutions as in PLA, Alexa Fluor 488 donkey anti-rabbit and Alexa Fluor 546 donkey anti-mouse secondary antibodies (1 : 100, A21206 and A10036, respectively; Invitrogen). After block permeation in PBS, 0.2% Triton X-100, 4% horse serum (for 20 min at room temperature), coverslips were incubated overnight at 4 °C in the primary antibodies (diluted in PBS, 0.1% Triton X-100, 4% horse serum) and after extensive washing in the secondary antibodies (diluted in PBS, 0.1% Triton X-100) for 1 h at room temperature. Coverslips were finally mounted using the Vectashield antifade mounting media (H-1700; Vector Laboratories). Stained coverslips were imaged using an inverted laser scanning confocal microscope (TCS SP5; Leica Microsystems, Wetzlar, Germany) equipped with a 63.0 × 1.25 NA plan apochromatic oil immersion objective. Confocal image stacks (10 sections each, optimised thickness) were acquired using the LEICA TCS software with a sequential mode to avoid interference between each channel due to spectral overlap and without saturating any pixel. Images were then prepared by superimposing the stacks acquired with the different channels. The presence of autofluorescence or nonspecific reactivity during imaging was ruled out taking as reference a sample incubated without specific primary antibodies (negative control). The signal/background noise ratio was adjusted by fixing the photomultiplier laser maximal levels of each channel, taking as reference the negative control prepared without specific primary antibodies.

The overlap between immunofluorescence signals corresponding to pairs of PP's enzymes, as well as their correlation, was analysed by the JACoP plugin in FIJI. Single images were processed by applying the median filter and subtracting the background (default parameters settings). Manders' coefficients were determined by adjusting the threshold of the green and red channels based on signals detected in single cells. The automatic Costes' threshold was selected during calculations of Pearsons' coefficients.

Acknowledgements

Conflict of interest

The authors declare no conflict of interest.

Author contributions

LP, AM and BC designed the project and conceptualised the approach; LP, BC, AP and SB supervised the project; VR performed chromatographic analyses and cross-linking experiments; FM and BC performed native PAGE analyses; FM, GM and LP performed kinetic analyses; SS performed cellular studies. All the authors performed data curation and wrote the original draft; VR, GM and FM prepared illustrations. All authors have read and agreed to the published version of the manuscript.

Data availability statement

The data that support the findings of this study are available from the corresponding authors (barbara.campanini@unipr.it; pollegioni@uninsubria.it) upon reasonable request.

References

1 Kawakami Y, Yoshida K, Yang JH, Suzuki T, Azuma N, Sakai K, Hashikawa T, Watanabe M, Yasuda K, Kuhara S *et al.* (2009) Impaired neurogenesis in embryonic spinal cord of Phgdh knockout mice, a serine deficiency disorder model. *Neurosci Res* **63**, 184–193.

2 Sayano T, Kawakami Y, Kusada W, Suzuki T, Kawano Y, Watanabe A, Takashima K, Arimoto Y, Esaki K, Wada A *et al.* (2013) L-serine deficiency caused by genetic Phgdh deletion leads to robust induction of 4E-BP1 and subsequent repression of translation initiation in the developing central nervous system. *FEBS J* **280**, 1502–1517.

3 Furuya S, Tabata T, Mitoma J, Yamada K, Yamasaki M, Makino A, Yamamoto T, Watanabe M, Kano M & Hirabayashi Y (2000) L-serine and glycine serve as major astroglia-derived trophic factors for cerebellar Purkinje neurons. *Proc Natl Acad Sci USA* **97**, 11528–11533.

4 Yamasaki M, Yamada K, Furuya S, Mitoma J, Hirabayashi Y & Watanabe M (2001) 3-Phosphoglycerate dehydrogenase, a key enzyme for L-serine biosynthesis, is preferentially expressed in the radial glia/astrocyte lineage and olfactory ensheathing glia in the mouse brain. *J Neurosci* **21**, 7691–7704.

5 Murtas G, Marcone GL, Sacchi S & Pollegioni L (2020) L-serine synthesis via the phosphorylated pathway in humans. *Cell Mol Life Sci* **77**, 5131–5148.

6 Chiba Y, Horita S, Ohtsuka J, Arai H, Nagata K, Igarashi Y, Tanokura M & Ishii M (2013) Structural units important for activity of a novel-type phosphoserine phosphatase from *Hydrogenobacter thermophilus* TK-6 revealed by crystal structure analysis. *J Biol Chem* **288**, 11448–11458.

7 Dubnovitsky AP, Kapetaniou EG & Papageorgiou AC (2005) Enzyme adaptation to alkaline pH: atomic resolution (1.08 A) structure of phosphoserine aminotransferase from *Bacillus alcalophilus*. *Protein Sci* **14**, 97–110.

8 Coulibaly F, Lassalle E, Baker HM & Baker EN (2012) Structure of phosphoserine aminotransferase from *Mycobacterium tuberculosis*. *Acta Crystallogr D* **68**, 553–563.

9 Ho CL, Noji M & Saito K (1999) Plastidic pathway of serine biosynthesis. Molecular cloning and expression of 3-phosphoserine phosphatase from *Arabidopsis thaliana*. *J Biol Chem* **274**, 11007–11012.

10 Sekula B, Ruszkowski M & Dauter Z (2018) Structural analysis of phosphoserine aminotransferase (isoform 1) from *Arabidopsis thaliana*- the enzyme involved in the phosphorylated pathway of serine biosynthesis. *Front Plant Sci* **9**, 876.

11 Ho CL, Noji M, Saito M, Yamazaki M & Saito K (1998) Molecular characterization of plastidic phosphoserine aminotransferase in serine biosynthesis from Arabidopsis. *Plant J* **16**, 443–452.

12 Neuhaus FC & Byrne WL (1959) Metabolism of phosphoserine. II. Purification and properties of O-phosphoserine phosphatase. *J Biol Chem* **234**, 113–121.

13 Paoli A, Guiraud P & Brunel C (1974) O-phosphoserine phosphatase from bovine brain and kidney. High molecular weight forms occurring during the purification. *Biochim Biophys Acta* **370**, 487–497.

14 Lund K, Merrill DK & Guynn RW (1987) Purification and properties of phosphoserine aminotransferase from bovine liver. *Arch Biochem Biophys* **254**, 319–328.

15 Basurko MJ, Marche M, Darriet M & Cassaigne A (1999) Phosphoserine aminotransferase, the second step-catalyzing enzyme for serine biosynthesis. *IUBMB Life* **48**, 525–529.

16 Hirsch H & Greenberg DM (1967) Studies on phosphoserine aminotransferase of sheep brain. *J Biol Chem* **242**, 2283–2287.

17 Grant GA (2018) D-3-phosphoglycerate dehydrogenase. *Front Mol Biosci* **5**, 110.

18 Tabatabaie L, Klomp LW, Rubio-Gozalbo ME, Spaapen LJ, Haagen AA, Dorland L & de Koning TJ (2011) Expanding the clinical spectrum of 3-phosphoglycerate dehydrogenase deficiency. *J Inherit Metab Dis* **34**, 181–184.

19 van der Crabben SN, Verhoeven-Duif NM, Brilstra EH, Van Maldergem L, Coskun T, Rubio-Gozalbo E,

Berger R & de Koning TJ (2013) An update on serine deficiency disorders. *J Inherit Metab Dis* **36**, 613–619.

20 El-Hattab AW, Shaheen R, Hertecant J, Galadari HI, Albaqawi BS, Nabil A & Alkuraya FS (2016) On the phenotypic spectrum of serine biosynthesis defects. *J Inherit Metab Dis* **39**, 373–381.

21 Amelio I, Cutruzzolá F, Antonov A, Agostini M & Melino G (2014) Serine and glycine metabolism in cancer. *Trends Biochem Sci* **39**, 191–198.

22 Maffioli E, Murtas G, Rabattoni V, Badone B, Tripodi F, Iannuzzi F, Licastro D, Nonnis S, Rinaldi AM, Motta Z *et al.* (2022) Insulin and serine metabolism as sex-specific hallmarks of Alzheimer's disease in the human hippocampus. *Cell Rep* **40**, 111271.

23 Nussinov R & Jang H (2014) Dynamic multiprotein assemblies shape the spatial structure of cell signaling. *Prog Biophys Mol Biol* **116**, 158–164.

24 Motlagh HN, Wrabl JO, Li J & Hilser VJ (2014) The ensemble nature of allostery. *Nature* **508**, 331–339.

25 Peracchi A & Mozzarelli A (2011) Exploring and exploiting allostery: models, evolution, and drug targeting. *Biochim Biophys Acta* **1814**, 922–933.

26 Kastritis PL & Gavin AC (2018) Enzymatic complexes across scales. *Essays Biochem* **62**, 501–514.

27 Castellana M, Wilson MZ, Xu Y, Joshi P, Cristea IM, Rabinowitz JD, Gitai Z & Wingreen NS (2014) Enzyme clustering accelerates processing of intermediates through metabolic channeling. *Nat Biotechnol* **32**, 1011–1018.

28 Bauler P, Huber G, Leyh T & McCammon JA (2010) Channeling by proximity: the catalytic advantages of active site colocalization using Brownian dynamics. *J Phys Chem Lett* **1**, 1332–1335.

29 An S, Kumar R, Sheets ED & Benkovic SJ (2008) Reversible compartmentalization of de novo purine biosynthetic complexes in living cells. *Science* **320**, 103–106.

30 An S, Deng Y, Tomsho JW, Kyoung M & Benkovic SJ (2010) Microtubule-assisted mechanism for functional metabolic macromolecular complex formation. *Proc Natl Acad Sci USA* **107**, 12872–12876.

31 Murtas G, Marcone GL, Peracchi A, Zangelmi E & Pollegioni L (2021) Biochemical and biophysical characterization of recombinant human 3-phosphoglycerate dehydrogenase. *Int J Mol Sci* **22**, 4231.

32 Marchesani F, Zangelmi E, Bruno S, Bettati S, Peracchi A & Campanini B (2021) A novel assay for phosphoserine phosphatase exploiting serine acetyltransferase as the coupling enzyme. *Life (Basel)* **11**, 485.

33 Marchesani F, Zangelmi E, Murtas G, Costanzi E, Ullah R, Peracchi A, Bruno S, Pollegioni L, Mozzarelli A, Storici P *et al.* (2023) L-serine biosynthesis in the human central nervous system: structure and function

of phosphoserine aminotransferase. *Protein Sci* **27**, e4609.

34 Söderberg O, Gullberg M, Jarvius M, Ridderstråle K, Leuchowius KJ, Jarvius J, Wester K, Hydbring P, Bahram F, Larsson LG *et al.* (2006) Direct observation of individual endogenous protein complexes in situ by proximity ligation. *Nat Methods* **3**, 995–1000.

35 Doigneaux C, Pedley AM, Mistry IN, Papayova M, Benkovic SJ & Tavassoli A (2020) Hypoxia drives the assembly of the multienzyme purinosome complex. *J Biol Chem* **295**, 9551–9566.

36 Pedley AM, Pareek V & Benkovic SJ (2022) The purinosome: a case study for a mammalian metabolon. *Annu Rev Biochem* **91**, 89–106.

37 Kohnhorst CL, Kyoung M, Jeon M, Schmitt DL, Kennedy EL, Ramirez J, Bracey SM, Luu BT, Russell SJ & An S (2017) Identification of a multienzyme complex for glucose metabolism in living cells. *J Biol Chem* **292**, 9191–9203.

38 Snell K & Fell DA (1990) Metabolic control analysis of mammalian serine metabolism. *Adv Enzyme Regul* **30**, 13–32.

39 Collet JF, Gerin I, Rider MH, Veiga-da-Cunha M & Van Schaftingen E (1997) Human L-3-phosphoserine phosphatase: sequence, expression and evidence for a phosphoenzyme intermediate. *FEBS Lett* **408**, 281–284.

40 Xu H, Qing X, Wang Q, Li C & Lai L (2021) Dimerization of PHGDH via the catalytic unit is essential for its enzymatic function. *J Biol Chem* **296**, 100572.

41 Fan J, Teng X, Liu L, Mattaini KR, Looper RE, Vander Heiden MG & Rabinowitz JD (2015) Human phosphoglycerate dehydrogenase produces the oncometabolite D-2-hydroxyglutarate. *ACS Chem Biol* **10**, 510–516.

42 Chan CY, Zhao H, Pugh RJ, Pedley AM, French J, Jones SA, Zhuang X, Jinnah H, Huang TJ & Benkovic SJ (2015) Purinosome formation as a function of the cell cycle. *Proc Natl Acad Sci USA* **112**, 1368–1373.

43 Pareek V, Sha Z, He J, Wingreen NS & Benkovic SJ (2021) Metabolic channeling: predictions, deductions, and evidence. *Mol Cell* **81**, 3775–3785.

44 Mishra V, Kumar A, Ali V, Nozaki T, Zhang KY & Bhakuni V (2012) Novel protein-protein interactions between *Entamoeba histolytica* D-phosphoglycerate dehydrogenase and phosphoserine aminotransferase. *Biochimie* **94**, 1676–1686.

45 Park JS, Burckhardt CJ, Lazcano R, Solis LM, Isogai T, Li L, Chen CS, Gao B, Minna JD, Bachoo R *et al.* (2020) Mechanical regulation of glycolysis via cytoskeleton architecture. *Nature* **578**, 621–626.

46 Laursen T, Møller BL & Bassard JE (2015) Plasticity of specialized metabolism as mediated by dynamic metabolons. *Trends Plant Sci* **20**, 20–32.

47 Perkins JR, Diboun I, Dessailly BH, Lees JG & Orengo C (2010) Transient protein-protein interactions:

structural, functional, and network properties. *Structure* **18**, 1233–1243.

48 Ma C, Zheng K, Jiang K, Zhao Q, Sha N, Wang W, Yan M, Chen T, Zhao Y & Jiang Y (2021) The alternative activity of nuclear PHGDH contributes to tumour growth under nutrient stress. *Nat Metab* **3**, 1357–1371.

49 Peeraer Y, Rabijns A, Collet JF, Van Schaftingen E & De Ranter C (2004) How calcium inhibits the magnesium-dependent enzyme human phosphoserine phosphatase. *Eur J Biochem* **271**, 3421–3427.

50 Fredriksson S, Gullberg M, Jarvius J, Olsson C, Pietras K, Gústafsdóttir SM, Ostman A & Landegren U (2002) Protein detection using proximity-dependent DNA ligation assays. *Nat Biotechnol* **20**, 473–477.

51 Yan SD, Fu J, Soto C, Chen X, Zhu H, Al-Mohanna F, Collison K, Zhu A, Stern E, Saido T *et al.* (1997) An intracellular protein that binds amyloid-beta peptide and mediates neurotoxicity in Alzheimer's disease. *Nature* **389**, 689–695.

52 Potokar M, Morita M, Wiche G & Jorgačevski J (2020) The diversity of intermediate filaments in astrocytes. *Cell* **9**, 1604.

53 Nakayama Y, Kinoshita A & Tomita M (2005) Dynamic simulation of red blood cell metabolism and its application to the analysis of a pathological condition. *Theor Biol Med Model* **2**, 18.

54 Zhu XH, Lu M, Lee BY, Ugurbil K & Chen W (2015) In vivo NAD assay reveals the intracellular NAD contents and redox state in healthy human brain and their age dependences. *Proc Natl Acad Sci USA* **112**, 2876–2881.

55 Zupke C, Sinskey AJ & Stephanopoulos G (1995) Intracellular flux analysis applied to the effect of dissolved oxygen on hybridomas. *Appl Microbiol Biotechnol* **44**, 27–36.

56 Molina JA, Jiménez-Jiménez FJ, Gomez P, Vargas C, Navarro JA, Ortí-Pareja M, Gasalla T, Benito-León J, Bermejo F & Arenas J (1997) Decreased cerebrospinal fluid levels of neutral and basic amino acids in patients with Parkinson's disease. *J Neurol Sci* **150**, 123–127.